

Numerical interactions between compactons and kovatons of the Rosenau-Pikovsky $K(\cos)$ equation

Julio Garralón, Francisco Rus, Francisco R. Villatoro

*Departamento de Lenguajes y Ciencias de la Computación,
Universidad de Málaga, Campus de Teatinos, 29071 Málaga, Spain*

Abstract

A numerical study of the nonlinear wave solutions of the Rosenau-Pikovsky $K(\cos)$ equation is presented. This equation supports at least two kind of solitary waves with compact support: *compactons* of varying amplitude and speed, both bounded, and *kovatons* which have the maximum compacton amplitude, but arbitrary width. A new Padé numerical method is used to simulate the propagation and, with small artificial viscosity added, the interaction between these kind of solitary waves. Several numerically induced phenomena that appear while propagating these compact travelling waves are discussed quantitatively, including self-similar forward and backward wavepackets. The collisions of compactons and kovatons show new phenomena such as the inversion of compactons and the generation of pairwise ripples decomposing into small compacton-anticompacton pairs.

Key words: $K(\cos)$ equation, Padé approximants, Numerical methods, Compactons, Kovatons, Solitary wave interactions
2000 MSC: 35Q51, 81T80

1 Introduction

Compactons are compactly-supported solitary waves that appear as solutions of some generalizations of the Korteweg–de Vries (KdV) equation characterized by the presence of nonlinear dispersion. Compactons were introduced for

* Corresponding author: villa@lcc.uma.es (Francisco R. Villatoro).

Email addresses: jgarralon@uma.es (Julio Garralón), rusman@lcc.uma.es (Francisco Rus), villa@lcc.uma.es (Francisco R. Villatoro).

the first time by Rosenau and Hyman [1] as solutions of the $K(m, n)$ equation, given by

$$\frac{\partial u}{\partial t} + \frac{\partial u^m}{\partial x} + \frac{\partial^3 u^n}{\partial x^3} = 0, \quad (1)$$

where x is the spatial variable and t is time, for certain values of m and n , and generalized by Khare and Cooper [2] for $n = m$. This kind of solitary waves presents some fundamental similarities with the *solitons* of the KdV equation, including the almost elastic interaction between them, but the non-linear dispersion in the $K(m, n)$ equation makes compactons quite a distinct mathematical object with its own properties [3,4], being its compact support the most important.

Numerical analysis has proved to be essential in the study of equations with compactly supported solitary waves. Pseudospectral [1,5], finite differences [6,7], Petrov-Garlerkin finite elements [8,9,10], Padé [11,12], and particle methods [5] have been used with more or less success. However, the numerical simulation of nonlinear travelling waves presents several numerically induced phenomena such as spurious radiation, artificial dissipation, or errors in group velocity, and the numerical evolution of compactons, especially at the edges of the support, is not free of these undesired effects [8,13]. Special attention has to be paid to the behaviour of compactons under mutual collisions, a key property to check for their robustness [13,14,15]. Although there is a large number of non-linear partial differential equations presenting compactly-supported solitary wave solutions [16], only a few have been numerically studied in detail.

Pikovsky and Rosenau [17] introduced a generalization of the $K(n, n)$ equation for the study of the quasicontinuous approximation of a one-dimensional lattice of coupled limit-cycle oscillators. Let us summarize the derivation presented in Refs. [18,19]. The k -th self-sustained oscillator with frequency ω is characterized by a phase ϕ_k that obeys $d\phi_k/d\tau = \omega$, where τ is time. Under weakly coupling, the equations for the phase differences read

$$\frac{d\phi_k}{d\tau} = \omega + q(\phi_{k-1} - \phi_k) + q(\phi_{k+1} - \phi_k),$$

where q is the coupling function, even and 2π -periodic in its argument. Introducing the variable $u_k = \phi_{k+1} - \phi_k$, the phase equations can be written as

$$\frac{du_k}{d\tau} = q(u_{k+1}) - q(u_{k-1}), \quad (2)$$

whose quasicontinuous approximation yields

$$\frac{\partial u}{\partial \tau} = 2h \frac{\partial(q(u))}{\partial y} + 2 \frac{h^3}{3!} \frac{\partial^3(q(u))}{\partial y^3} + O(h^5),$$

where h is the spatial step of the lattice. Neglecting higher order terms and applying a change of variables, this equation can be non-dimensionalized to

$$\frac{\partial u}{\partial t} = \frac{\partial q(u)}{\partial x} + \frac{\partial^3 q(u)}{\partial x^3}. \quad (3)$$

For $q(u) = -\cos(u)$ we obtain the so-called $K(\cos)$ equation, given by

$$\frac{\partial u}{\partial t} + \frac{\partial \cos(u)}{\partial x} + \frac{\partial^3 \cos(u)}{\partial x^3} = 0, \quad (4)$$

that admits compactly-supported travelling waves such as compactons, kinks, and what Pikovsky and Rosenau referred to as *kovatons*, which result from gluing together a kink-antikink pair with a plateau of arbitrary width.

The closed form expression for the shape of compactons and kovatons of the $K(\cos)$ equation is not known in closed form [18,20]. Its determination by means of numerical methods requires the solution of a nonlinear eigenvalue problem [21]. Recently, Garralón and Villatoro [22] proposed a procedure for the numerical quadrature of the solitary waves of the $K(\cos)$ equation, which can be used as initial conditions for compactons and kovatons numerical evolution. These solutions are only characterized by one parameter, the velocity c of the solitary wave. The nonlinear relation between the amplitude and velocity of compactons must be numerically determined.

The behaviour of compactons (and antcompactons) of the $K(\cos)$ equation differs from those of the $K(2,2)$ equation in several aspects [22]. Firstly, the absolute value of their velocity is upper bounded by $c_{\max} = 2/\pi$, the velocity of the kovatons (and antikovatons), whereas for the $K(2,2)$ there is no upper bound. Secondly, compactons (antcompactons) propagates to the left (right), i.e., to minus (plus) infinity in x , and the opposite occurs for those of the $K(2,2)$. And thirdly, the width of the $K(\cos)$ compactons increases as it does the absolute value of the velocity, as shown in Fig. 1, while it is independent of the velocity for the $K(2,2)$ ones.

The $K(\cos)$ equation has several applications in physical problems such an array of superconducting Josephson junctions [23] and the spontaneous otoacoustic emissions in the inner ear of certain lizards [24]. Let us also note that compact kinks are the solutions of nonlinear evolution equations modelling several applications such as waves in viscoelastic solids [25], double-stranded

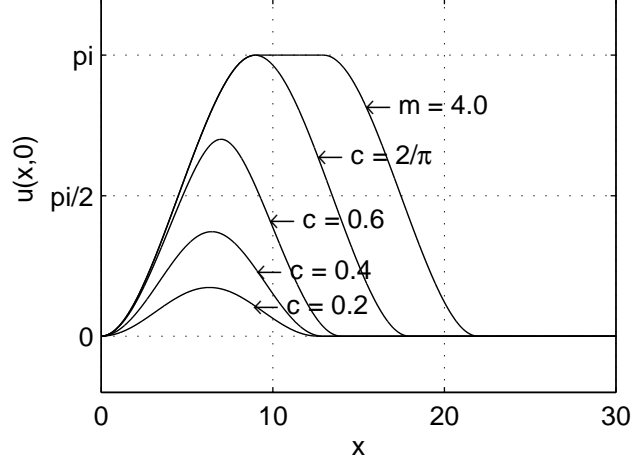


Fig. 1. Compactons of the $K(\cos)$ equation with speeds $c = 0.2, 0.4, 0.6$, and $2/\pi$, and a kovaton with plateau length $m = 4.0$.

DNA molecules [26], and nonlinear electrical transmission lines [27], to mention only a few.

The contents of this paper are as follows. Next section presents a new numerical scheme used to solve the $K(\cos)$ equation, based on Padé approximants in space and a method of lines in time. Both compactons and kovatons have been studied, analyzing the residual structures that appear when propagating them alone as well as after pairwise interactions in Section 3. Finally, the last section is devoted to some conclusions.

2 Numerical method

Let us consider a method of lines in time and a Padé approximation method in space with periodic boundary conditions [12] for solving Eq. (4) numerically. Taking a fixed grid spacing Δx , the $M+1$ spatial nodes of the interval $x \in [0, L]$ are $x_j = j \Delta x$, for $j = 0, 1 \dots M$, and the Padé method is written as

$$\mathcal{A}(E) \frac{dU_j}{dt} + c_0 \mathcal{B}(E) U_j + (\mathcal{B}(E) + \mathcal{C}(E)) \cos(U_j) = 0, \quad (5)$$

where $U_j(t) \approx u(x_j, t)$, E is the shift operator, i.e., $E U_j = U_{j+1}$, and the first and third derivatives are rationally approximated by means of $\mathcal{B}(E)/\mathcal{A}(E)$ and $\mathcal{C}(E)/\mathcal{A}(E)$, respectively, where

$$\mathcal{A}(E) = \frac{E^{-2} + 26 E^{-1} + 66 + 26 E^1 + E^2}{120},$$

$$\mathcal{B}(E) = \frac{-E^{-2} - 10 E^{-1} + 10 E^1 + E^2}{24 \Delta x},$$

$$\mathcal{C}(E) = \frac{-E^{-2} + 2 E^{-1} - 2 E^1 + E^2}{2 \Delta x^3}.$$

The numerical method (5) is fourth-order accurate in space for regular enough solutions ($u(x, t) \in C^7$), since its truncation error terms are given by

$$\text{TET}\{u(x, t)\} = \frac{\Delta x^4}{240} \frac{\partial^7}{\partial x^7} \cos(u) + O(\Delta x^6).$$

It should be noted that the Padé numerical method (5) is a fourth-order approximation in Δx to the continuous equation (4), which in turn is a fourth-order approximation in h to the discrete equation (2). Although, Δx and h can be related by a proper scaling, physically it has no sense, since h is a fixed parameter of the original discrete model, but Δx is a tunable numerical parameter.

In solutions of the $K(\cos)$ equation with multiple colliding compactons and kovatons, ripples (or nonsmooth solutions) are developed reducing the effective order of accuracy and introducing numerical instabilities which may blow up the solution [8,11,13]. In order to avoid these instabilities, an artificial viscosity term, $\mu \partial^4 u / \partial x^4$, with μ small enough, must be introduced into the non-dissipative method given by Eq. (5) and numerically discretized by means of a second-order accurate five-point difference formula, given by

$$\mathcal{D}(E) U_j = \frac{E^{-2} - 4 E^{-1} + 6 - 4 E^1 + E^2}{\Delta x^4} U_j. \quad (6)$$

Note that the addition of the artificial viscosity reduces the order of consistency of the method down to the second, resulting in

$$\text{TET}_{\mathcal{D}}\{u(x, t)\} = \frac{\Delta x^2}{6} \frac{\partial^6 u}{\partial x^6} + O(\Delta x^4).$$

The second-order implicit midpoint rule is used for the integration in time, yielding

$$\begin{aligned} \mathcal{A}(E) \frac{U_j^{m+1} - U_j^m}{\Delta t} + (\mu \mathcal{D}(E) + c_0 \mathcal{B}(E)) \left(\frac{U_j^{m+1} + U_j^m}{2} \right) \\ + (\mathcal{B}(E) + \mathcal{C}(E)) \cos \left(\frac{U_j^{m+1} + U_j^m}{2} \right) = 0, \end{aligned} \quad (7)$$

c	$\Delta x, \quad \Delta t = 0.001$				
	0.1	0.05	0.01	0.005	0.001
$1/2$	7.9×10^{-6}	3.5×10^{-6}	6.1×10^{-7}	1.2×10^{-6}	—
$2/\pi$	1.6×10^{-5}	8.0×10^{-6}	3.0×10^{-6}	4.5×10^{-6}	—

c	$\Delta x = 0.1, \quad \Delta t$				
	0.1	0.05	0.01	0.005	0.001
$1/2$	7.7×10^{-6}	7.8×10^{-6}	8.7×10^{-6}	8.1×10^{-6}	7.9×10^{-6}
$2/\pi$	1.0×10^{-5}	1.4×10^{-5}	1.6×10^{-5}	1.6×10^{-5}	1.6×10^{-5}

Table 1

Numerical errors in infinite norm for the one-compacton solution of the $K(\cos)$ equation at $t = 20$ as a function of Δx and fixed $\Delta t = 0.001$ (top), and as a function of Δt and fixed $\Delta x = 0.1$ (bottom), using $L = 150$, $\mu = 0$, and $c_0 = c$.

where U_j^m is an approximation to $u(x_j, t^m)$, with $t^m = m \Delta t$.

3 Presentation of results

Extensive numerical experiments with the above scheme has proved to be good in accuracy and conservation properties for both $\mu = 0$ and, when required, a small properly chosen μ . Let us summarize the results in the following subsections.

3.1 One-compacton solution

Let us consider the numerical simulation of the propagation of one compacton of the $K(\cos)$ equation calculated by method (7) without artificial viscosity ($\mu = 0$), stopped in the integration interval by setting $c_0 = c$.

Table 1 shows the error in infinite norm between the exact one-compacton solution (determined as described in Ref. [22] with machine precision) and the numerical one at $t = 20$, i.e., $\max_j |U_j(20) - u(x_j, 20)|$, as a function of Δx (top) and Δt (bottom). For $\Delta x \geq 0.01$ and $\Delta t = 0.001$, Table 1 shows that the numerical error decreases as Δx does for compactons with velocities $c = 0.5$ and $c = 2/\pi$ (the highest one). For $\Delta x < 0.01$ the error is higher for $\Delta x \leq 0.001$ the solution blows up even for a stopped compacton (indicated as — in the table); apparently this behaviour is surprising since the CFL (Courant-Friedrichs-Lewy) condition ($\Delta x/\Delta t \geq c - c_0 = 0$) is always met. However, the CFL condition for the numerically induced wavepackets

c	$\Delta x, \quad \Delta t = 0.001$				
	0.1	0.05	0.01	0.005	0.001
$1/2$	1.4×10^{-13}	2.4×10^{-12}	9.5×10^{-10}	2.9×10^{-9}	—
$2/\pi$	2.9×10^{-13}	1.5×10^{-11}	1.2×10^{-9}	2.6×10^{-9}	—

c	$\Delta x = 0.1, \quad \Delta t$				
	0.1	0.05	0.01	0.005	0.001
$1/2$	1.7×10^{-12}	1.0×10^{-12}	1.4×10^{-13}	1.5×10^{-12}	4.7×10^{-13}
$2/\pi$	7.1×10^{-15}	1.1×10^{-12}	2.3×10^{-12}	9.7×10^{-13}	2.9×10^{-13}

Table 2

Numerical error for the second invariant I_2 for the one-compacton solution of the $K(\cos)$ at $t = 20$, as a function of Δx and fixed $\Delta t = 0.001$ (top), and as a function of Δt and fixed $\Delta x = 0.1$ (bottom), using $L = 150$, $\mu = 0$, and $c_0 = c$.

of radiation, to be studied later in this section, does not holds, hence an instability develops. On the other hand, Table 1 (bottom) shows that the error for both compactons is practically independent of Δt , and no problems of stability due to the CFL condition arise. Finally, let us note that the behaviour of the errors for antcompactons is the same as that for compactons with the same parameters (except that $c_0 = -c$ must be used to stop them in the numerical frame).

The numerical method used in this paper preserves exactly the first invariant for the $K(\cos)$ equation with $\mu = 0$, i.e.,

$$I_1 = \int_{-\infty}^{\infty} u(x, t) dx,$$

since by summing in space it may be easily shown that $\sum_m u_m^n = \sum_m u_m^0$. However, second invariant

$$I_2 = \int_{-\infty}^{\infty} \sin(u(x, t)) dx$$

is not exactly preserved. This invariant has been numerically calculated by means of the trapezoidal quadrature rule.

Table 2 shows the error of the second invariant for one-compacton solution at $t = 20$ as a function of Δx (top) and Δt (bottom), i.e., $|I_2(20) - I_2(0)|$. As shown in this table, the error grows as Δx decreases for compactons with both velocities $c = 0.5$ and $c = 2/\pi$, except in the case with the lowest Δx

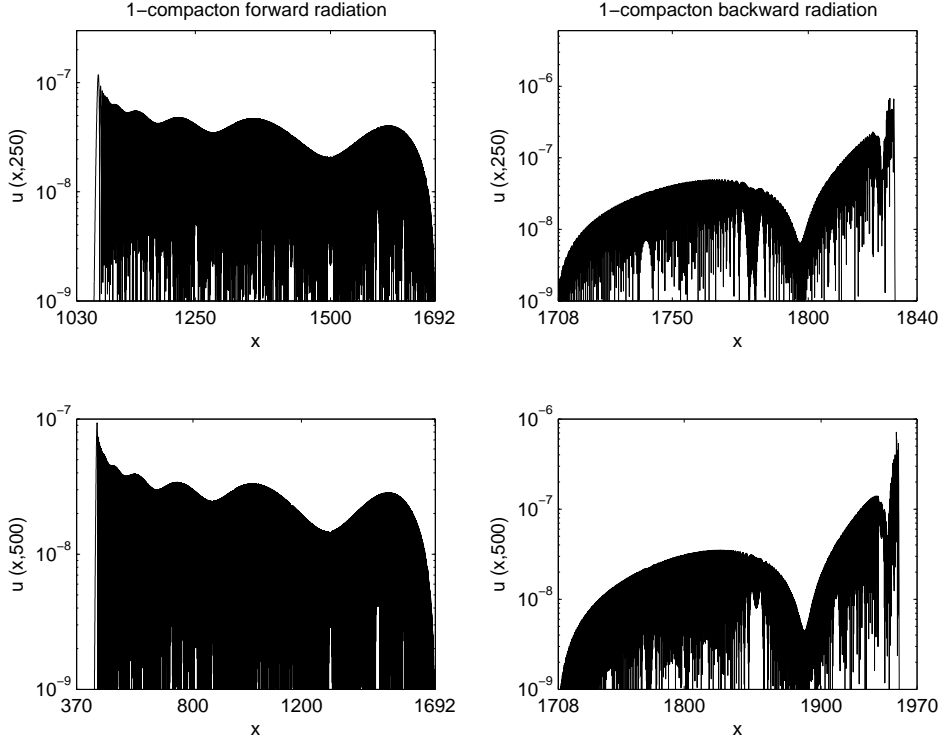


Fig. 2. Forward (left plots) and backward (right plots) radiations generated during a compacton propagation with $c = 0.5$, $\Delta x = 0.05$, $\Delta t = 0.01$, and $\mu = 0$, at time $t = 250$ (top plots) and $t = 500$ (bottom plots), highlighting their self-similarity.

for $c = 2/\pi$. By contrast, Table 2 (bottom) shows that the error of the second invariant is practically constant, nearly independent of Δt .

The numerical evolution of compactons of the $K(\cos)$ equation shows the presence of two numerically-induced small amplitude wavepackets, one propagating to the left, the *forward radiation*, and the other one to the right, the *backward radiation* (recall that compactons travel to the left). Extensive numerical experiments show that the velocities of the wavefront for both the backward and forward radiation are independent of Δx and Δt parameters. On the other hand, the amplitude of radiations emitted for compactons increases as so do Δx and c .

Another worth noting fact is that the radiations shape is self-similar, as in the Rosenau-Hyman $K(2, 2)$ equation case reported in Ref. [13]. Both the forward and backward wavepackets present this self-similarity regardless of parameters Δx and Δt . Figure 2 clearly shows this property with plots of the radiations at two different times, stretching the horizontal axis in order to highlight the self-similarity.

Similar results have been obtained for compactons with different amplitudes in long time simulations, enlarging the computational interval in order to

$\Delta x/\Delta t$	$c = 1/2$		$c = 2/\pi$	
	c_f	$-c_b$	c_f	$-c_b$
0.5	2.511	0.4938	3.218	0.6362
5	2.511	0.4989	3.209	0.6360
50	2.511	0.4985	3.209	0.6362

Table 3

Front speeds of both the backward (c_b) and forward (c_f) radiation relative to that of a compacton with speeds $c = 1/2$ and $c = 2/\pi$. The parameters used are $\Delta x = 0.05$, $L = 300$ and $c_0 = c$.

avoid that the wavepackets overlap due to the periodicity of the boundary conditions.

Table 3 shows the front speed of the forward (c_f) and backward (c_b) wavepackets of radiation relative to that of two compactons with speeds $c = 0.5$ and $c = 2/\pi$. These speeds have been calculated by using linear regression of the position of the wavefronts in time, calculated by using a threshold equal to the half of the maximum amplitude of the radiation in the integration interval (the same procedure used in Ref. [13]). Table 3 shows that both the forward (c_f) and backward (c_b) front velocities are nearly constant (independent of both Δt and Δx) being $c_f \approx 5c$ and $c_b \approx -c$.

Due to the fact that the forward speed c_f is five times faster than that of a compacton, care must be taken when setting parameters Δx and Δt in order to meet the CFL condition, so that $\Delta x/\Delta t \geq c_f \approx 5c$. This could be the reason of the blow up in the simulations of the last column of Tables 1 and 2 (top).

3.2 One-kovaton solution

Let us consider the numerical simulation of the propagation of one kovaton of the $K(\cos)$ equation calculated by method (7) without artificial viscosity ($\mu = 0$), stopped in the integration interval by setting $c_0 = c$.

Table 4 shows the error in infinite norm between the exact one-kovaton solution and the numerical one at $t = 150$ as a function of the plateau size m . The error is nearly constant for $m < 4$, but grows linearly for $m \geq 4$; in fact, a linear regression shows that, in such a case, the error is equal to $(4.1m - 0.49) \times 10^{-6}$. Table 4 also shows that the error in the second invariant is very small and nearly independent of m .

The linear behaviour of the error for a kovaton with $m \geq 4$ shown in Table 4

m	$\ U(150) - u(\cdot, 150)\ _\infty$	$ I_2(150) - I_2(0) $
0.1	7.45×10^{-6}	3.75×10^{-10}
0.4	1.50×10^{-5}	7.43×10^{-10}
0.6	1.42×10^{-5}	8.23×10^{-10}
1	1.43×10^{-5}	4.75×10^{-9}
4	1.58×10^{-5}	2.81×10^{-9}
6	2.40×10^{-5}	7.16×10^{-11}
10	4.03×10^{-5}	1.33×10^{-9}
40	1.62×10^{-4}	1.06×10^{-9}
60	2.44×10^{-4}	2.58×10^{-9}

Table 4

Numerical errors in infinite norm for the one-kovaton solution of the $K(\cos)$ equation at $t = 150$ and for the second invariant as a function of the plateau size m , using $\Delta x = 0.05$, $\Delta t = 0.01$, $L = 220$, $\mu = 0$, and $c_0 = c_{\max}$.

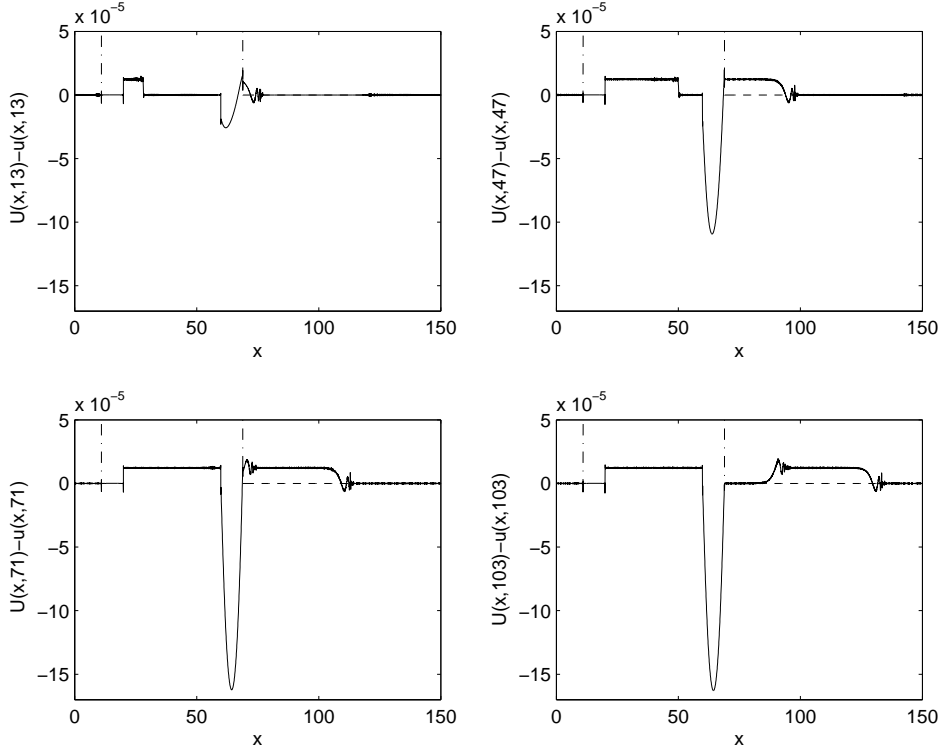


Fig. 3. Evolution in time of the numerical error during one-kovaton propagation for $t = 13$ (top left plot), $t = 47$ (top right one), $t = 71$ (bottom left one), and $t = 103$ (bottom right one), with $m = 60$, $\Delta x = 0.05$ and $\Delta t = 0.01$, $c_0 = 0$, and $\mu = 0$.

is due to the appearance of a peak in its backward kink whose amplitude is dependent only on the value of m , as illustrated in Fig. 3. The evolution of the error presents three main features occurring simultaneously with the propagation of the kovaton, whose edges correspond to the vertical, broken-and-dotted lines in Fig. 3. First, a square pulse appears on the flat-top of the kovaton (Fig. 3, top left plot), whose right front propagates from the forward kink to the backward one with the kovaton's speed (Fig. 3, top right plot) until the kovaton has advanced a distance equal to m (Fig. 3, bottom left plot); here on, the shape of the square pulse remains constant without changes (Fig. 3, bottom right plot). Second, a downward peak appears at the position of the backward kink (Fig. 3, top left plot), whose amplitude grows until reaching a maximum value when the square pulse has passed through the flat-top (Fig. 3, bottom left plot); from this point on, the shape of the peak remains constant. And third, another square-like pulse, but with dispersive fronts at both edges, appears behind the kovaton (Fig. 3, top right plot) and propagates to the right, growing in width until it equals the length of the plateau, when it leaves the backward kink (Fig. 3, bottom right plot). The conservation of the first invariant of the $K(\cos)$ equation implies that the total area of the peak is equal to the sum of the areas of both square pulses.

Kovaton propagation is also accompanied by two self-similar wavepackets of radiation whose shape is very similar to that of the one-compacton solution with maximum speed (cf. Fig. 2). The front speed of the forward (c_f) and backward (c_b) wavepackets of radiation are nearly constant, independent of both Δt , Δx , and the width m of the plateau, being approximately equal to $c_f \approx 5c$ and $c_b \approx -c$.

3.3 Compacton and kovaton collisions

The numerical evolution of compactons and kovatons interactions is a more subtle problem than that of propagating them alone due to the large slopes developed, and a stable method for one-compacton or one-kovaton evolution may become unstable in mutual interaction. In fact, without artificial viscosity, $\mu = 0$, the numerical method blows up during any kind of interaction between them. On the other hand, artificial dissipation greater than zero generates tails and lags distorting the original signal. Numerical experimentation has proved a value of $\mu = 10^{-3}$ to be adequate.

Figure 4 shows a sequence of plots with a collision between two compactons, one with speed $c_1 = 1/2$ (the left one in the first snapshot), stopped in the computational frame by taking $c_0 = c_1$, and the other one with the highest possible speed, $c_2 = 2/\pi$ (the right one in the same snapshot). Both compactons collide elastically reemerging with the same shape after the interaction with a

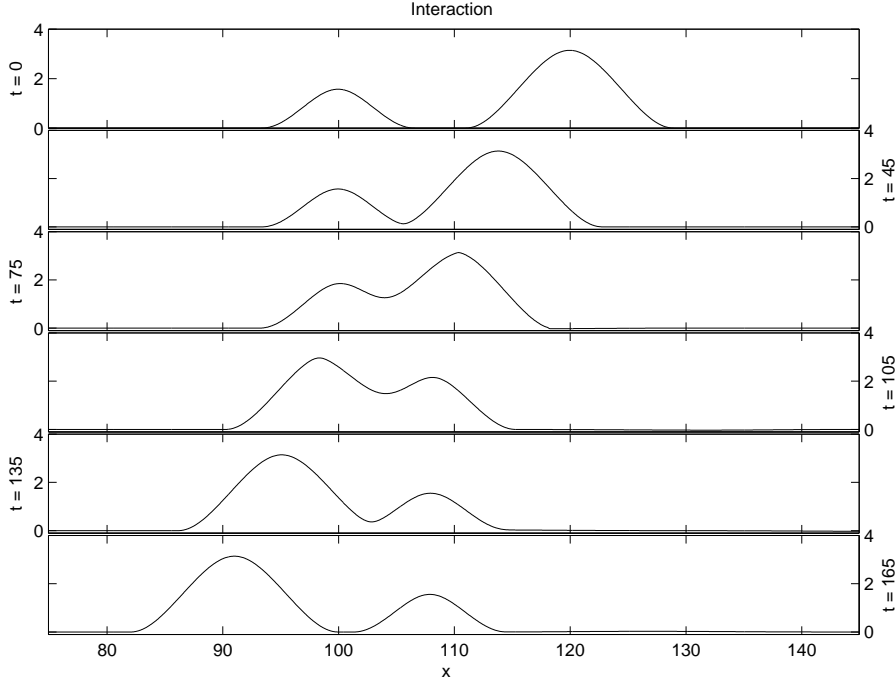


Fig. 4. Collision between two compactons with velocities $c_1 = 1/2$ (the left one in the first plot) and $c_2 = 2/\pi$ (the right one), using $\mu = 10^{-3}$, $c_0 = c_1$, $\Delta x = 0.05$ and $\Delta t = 0.01$.

small shift in their positions, the largest compacton suffering a positive shift to the left, and the smallest one a negative one to the right (let's compare the position of the smallest one between the top and bottom plots in Fig. 4). In addition, a residual (not shown in the plot due to its small amplitude) appears at the position of the interaction.

Figure 5 shows a interaction between a compacton with speed $c = 0.9 c_{\max}$ and a kovaton with plateau length $m = 40$. The compacton passes through the rising kink of the kovaton, then it reappears reversed (second snapshot in Fig. 5), travelling like an antcompacton along the plateau (fourth snapshot), until reaching the falling kink of the kovaton (sixth snapshot), when it reemerges with its original shape (seventh snapshot). Of course, this phenomenon can not be clearly observed if the size of the plateau of the kovaton is less than the width of the compacton. Note that the width of the signal during the collision is the sum of both the width of the compacton and the kovaton before the interaction. Also note the phase shift in the positions of both solitary waves after the interaction.

Compactons correspond to homoclinic orbits in the phase plane $(u(\cdot, t), u_x(\cdot, t))$, at the critical point $(0, 0)$, and kovatons to heteroclinic orbits between the critical points $(0, 0)$ and $(\pi, 0)$; the evolution in time of these orbits is a useful tool to study their interactions. Figure 6 shows the collision between a compacton with speed $c = 0.2$ and a kovaton with plateau length $m = 40$. The interaction

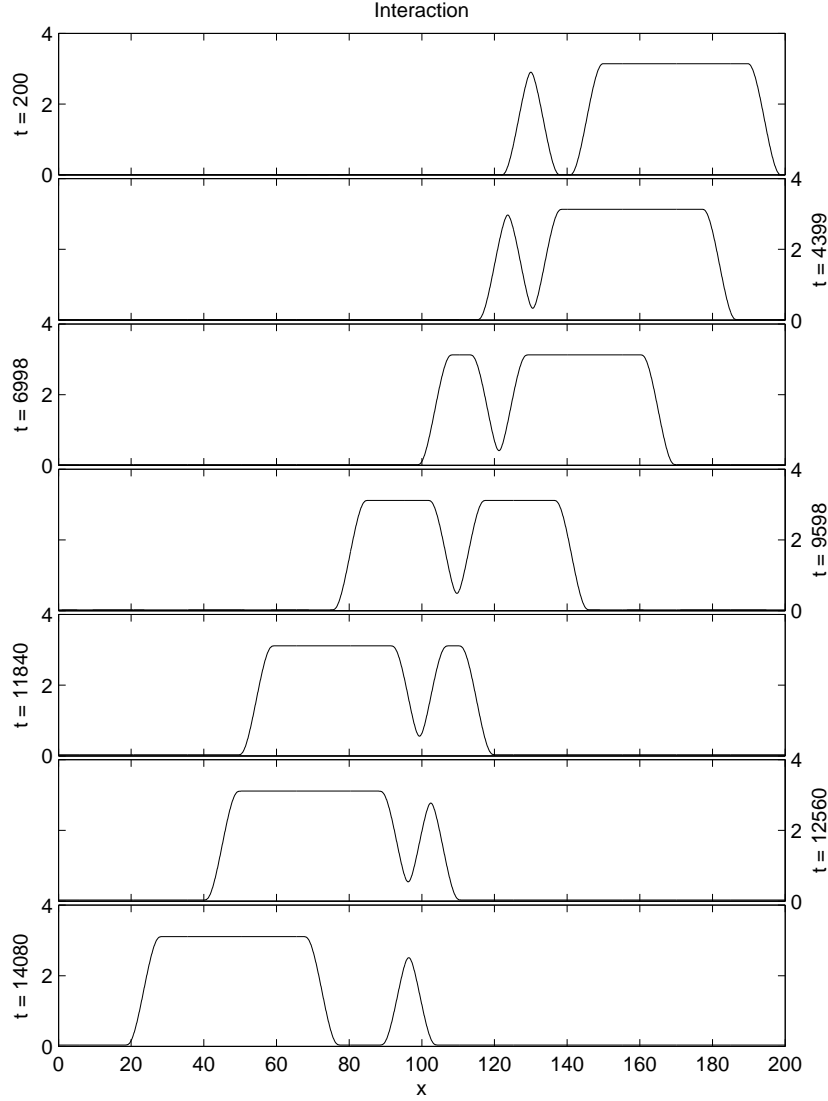


Fig. 5. Collision between a compacton with speed $c = 0.9c_{\max}$ and a kovaton with plateau $m = 40$, using $\mu = 10^{-3}$, $c_0 = c$, $\Delta x = 0.05$ and $\Delta t = 0.01$.

has actually three definite parts, the first being the entrance of the compacton into the kovaton, the second being the travelling of the compacton along the plateau of the kovaton, and the third being the exit of the compacton from the kovaton. In the top left plot of Fig. 6 the phase plane shows two ellipses, the largest one corresponding to the heteroclinic orbit of the kovaton and the smallest one to the homoclinic orbit of the compacton, both before the interaction begins. Next, the compacton enters the rising kink of the kovaton, corresponding to the left inner loop in the phase plane near the critical point

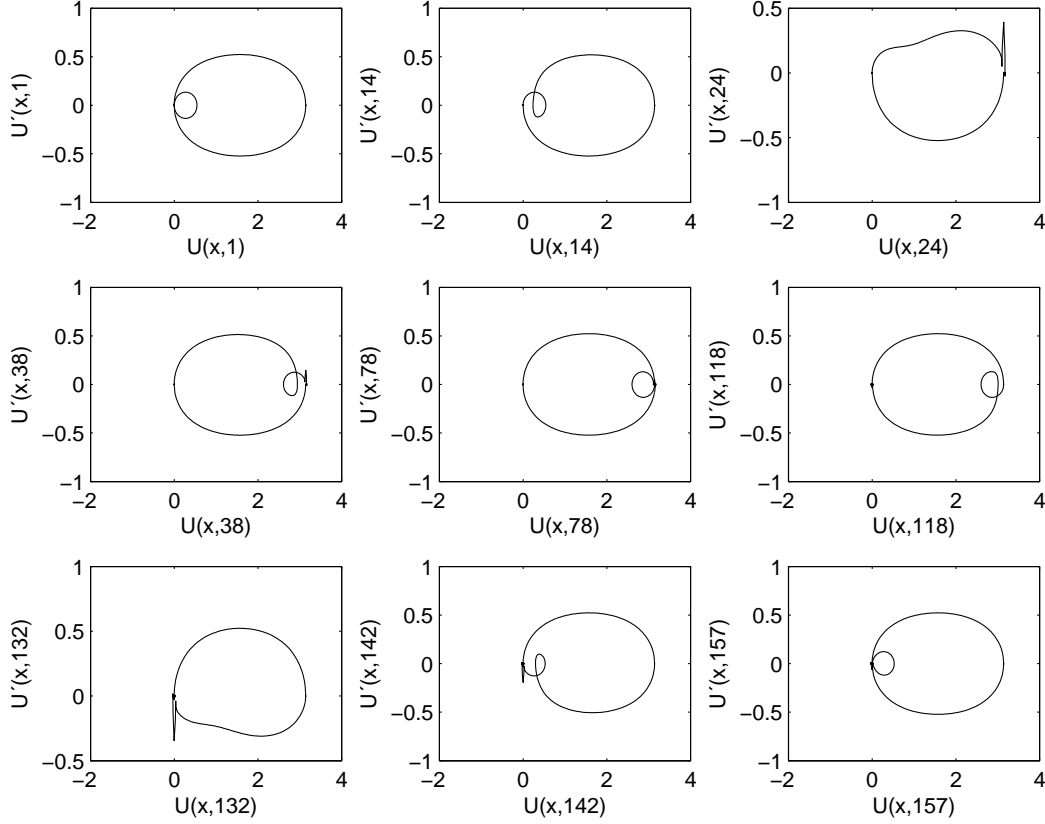


Fig. 6. Sequence of the phase plane of a collision between a compacton with speed $c = 0.2$ and a kovaton with plateau $m = 40$, with $\mu = 10^{-3}$, $c_0 = 2/\pi$, $x \in [0, 200]$, $\Delta x = 0.05$, and $\Delta t = 0.01$.

$(0, 0)$ (top center). When the compacton reaches the plateau of the kovaton, high slopes develop at the left side the plateau, causing the appearance of a sharp peak in the phase plane near $(\pi, 0)$ (top right). Then the compacton is almost completely inside the plateau of the kovaton, corresponding to the right inner loop in the phase plane near $(\pi, 0)$ (middle left). When the entrance of the compacton has finished, the compacton travels reversed all along the plateau of the kovaton, a remarkable situation that is plotted by two orbits in the phase plane, the smallest one corresponding now to an antcompacton on the plateau, and the largest one to the kovaton (middle center). When the compacton gets to the falling kink of the kovaton, it recovers its original shape and the phase plane plots the right inner loop at $(\pi, 0)$ first (middle right), the sharp peak at low amplitudes shortly afterwards (bottom left), the left inner loop at $(0, 0)$ (bottom center), and the final situation with the two original orbits (bottom right).

Another fact worth mentioning is the appearance of a zero-mass small amplitude ripple after every collision either between two compactons or between a compacton and a kovaton. Figure 7 zooms it for two compactons with velocities $c_1 = 0.5$ and $c_2 = 2/\pi$. The first plot shows the situation previous to

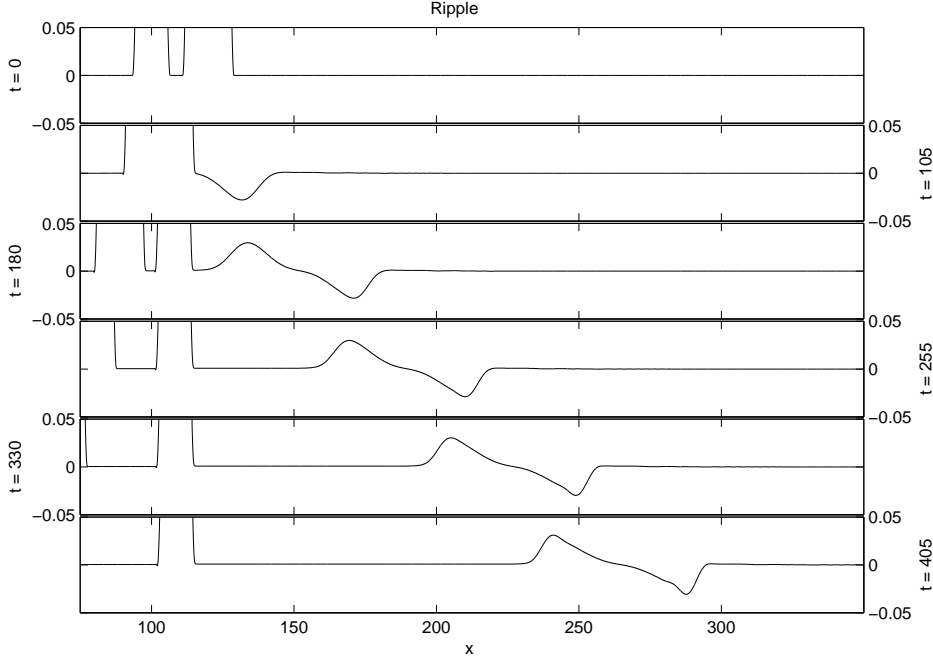


Fig. 7. Sequence of zooms of the evolution of the ripple developed after a collision between two compactons, one with speed $c_1 = 0.5$ (the left one in the first zoom) and the other one with speed $c_2 = 2/\pi$ (the right one in the same zoom), using $\mu = 10^{-3}$, $c_0 = 0.5$, $\Delta x = 0.05$, and $\Delta t = 0.01$.

the collision, with the faster (wider) compacton at the right. In the next plot we can see the birth of the ripple, only with its negative half part developed. The following plots show the evolution in time of this ripple, travelling to the right in the computational frame at a speed equal to c_0 , i.e., it remains at rest at the point where the collision begins. This ripple is similar to those appearing in numerical simulations of $K(2, 2)$ compactons, except for the fact that there are no sharp fronts inside (see [11]).

The residual appearing after a compacton-kovaton collision consists of two separated ripples, as depicted in Fig. 8 (top left plot), the first one corresponding to the collision of the compacton with the rising kink of the kovaton, labelled as a_1 and a_2 in the plot, and the second one corresponding to the interaction of the now antcompacton at the plateau of the kovaton with its falling kink, labelled as b_1 and b_2 . Thus, a_1 (a_2) appears during the interaction between the negative (positive) slope part of the compacton and the rising kink of the kovaton. After the first ripple is generated, the compacton travels reversed along the plateau, and then b_1 (b_2) appears during the interaction between the positive (negative) slope part of the now antcompacton and the falling kink of the kovaton. It should be noted that the distance between the two ripples equals the length of the plateau of the kovaton. In the following plots of the same figure, as the evolution progresses, the positive (negative) semi-ripples break down and decompose into trains of positive (negative) pulses of

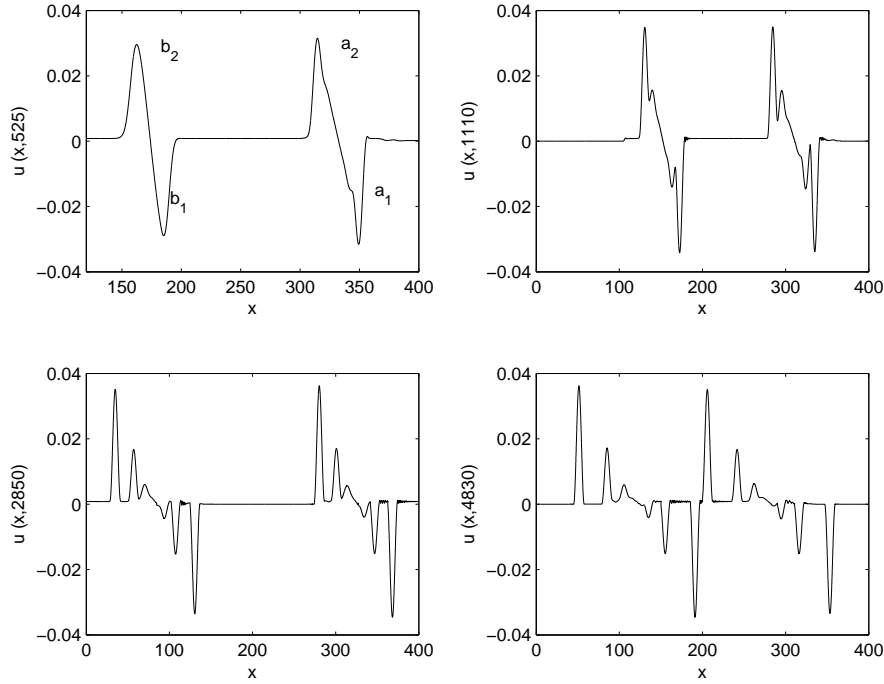


Fig. 8. Evolution of the ripples generated after a collision between a compacton with speed $c = 0.5$ and a kovaton with plateau length $m = 40$, using $\mu = 10^{-5}$, $\Delta x = 0.05$, $\Delta t = 0.01$, and $c_0 = 0$. The snapshots correspond to time $t = 525$, 1110 , 2850 , and 4830 .

decreasing amplitude, all of them with a width of 4π , corresponding to small amplitude compactons (antcompactons).

3.4 Compacton-antcompacton collisions

Collisions between compactons and antcompactons, even adding the artificial viscosity term, have proved to be unstable resulting in blow up, although extensive numerical simulations have shown that the behaviour of the numerical method for the propagation of antcompactons alone in terms of the error and the invariants is the same as that of compactons with the same speed, discussed in Section 3.1.

Figure 9 shows the collision between a compacton with speed $c_1 = 0.5$ and an antcompacton with $c_2 = -0.5$. The top plots are two snapshots previous to the collision. In the middle ones, zoomed in, unexpected high frequency phenomena that begin to occur at the external edges can be observed. Conversely, the solution is apparently smooth at the central part. The amplitude of these high frequency phenomena increases as the blow up time approaches as shown in the bottom left zoomed out plot. Finally, the last bottom right plot shows

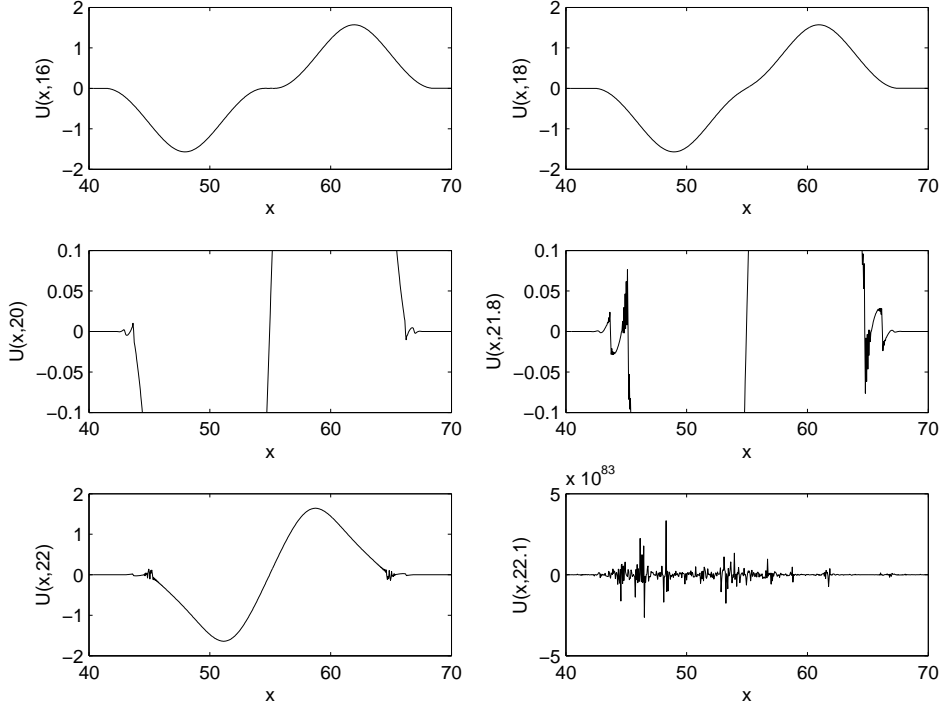


Fig. 9. Snapshots of a compacton-anticompacton collision, both with $|c| = 0.5$, at times $t = 16$ (top left plot), 18 (top right), 20 (middle left), 21.8 (middle right), 22 (bottom left), and 22.1 (bottom right), using $\Delta x = 0.05$, $\Delta t = 0.01$, $c_0 = 0$, and $\mu = 10^{-4}$.

the blow up.

Figure 10 shows the phase plane plots corresponding to the same snapshots shown in Fig. 9. The left homoclinic orbit (negative amplitudes) of the top left plot in Fig. 10 corresponds to the antcompacton, and the right one (positive amplitudes) to the compacton. The top right plot in Fig. 10 show that as the travelling waves approach each other, the slope of the solution increases at the position where the compacton and antcompacton first met. In the middle left plot of Fig. 10 a sharp peak in the bottom part of the melted orbits can also be observed, corresponding to the high frequency phenomena that begin to develop at the external edges of both travelling waves shown in Fig. 9 (middle left plot). These high frequency phenomena increase at the external edges causing the peak to grow in the phase plane as depicted in in Fig. 10 (middle right and bottom left plots). The final bottom right plot makes evident the blow up.

The blow up during the compacton-anticompacton collision is due to the development of dispersive shock-like phenomena of increasing amplitude which appears in the regions of the solution with negative slope. Figure 11 (left plot) shows the solution for $\mu = 10^{-4}$ a few time steps before blow up; the use of a larger artificial viscosity (right plot) simply delays the blow up. The four

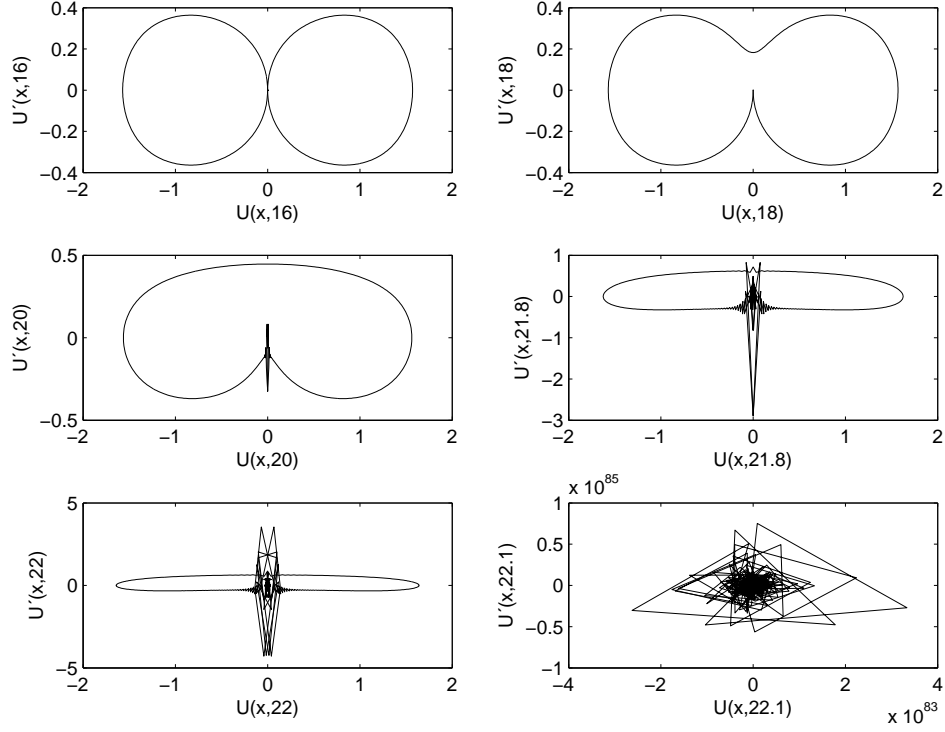


Fig. 10. Sequence of phase plane plots of a compacton-anticompacton collision both with $|c| = 0.5$ at times $t = 16$ (top left plot), 18 (top right), 20 (middle left), 21.8 (middle right), 22 (bottom left), and 22.1 (bottom right), using $\Delta x = 0.05$, $\Delta t = 0.01$, $c_0 = 0$, and $\mu = 10^{-4}$.

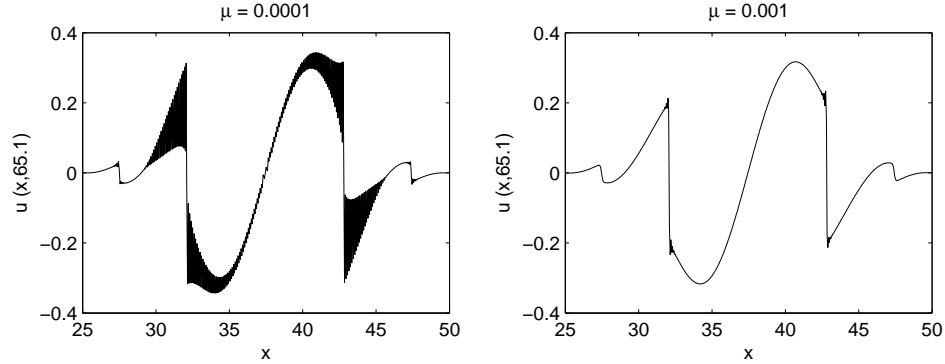


Fig. 11. A compacton-anticompacton collision both with $|c| = 0.5$ at time $t = 65.1$ with $\mu = 10^{-4}$ (left plot) and 10^{-3} (right one), using $\Delta x = 0.05$, $\Delta t = 0.01$, and $c_0 = 0$.

shocks shown in Fig. 11 present high frequency dispersion whose amplitude grows up as blow up time approaches. Our numerical simulations show that these phenomena is robust to changes in the parameters of the numerical method, Δx and Δt , indicating its possible origin in the analytical behaviour of the solutions of the $K(\cos)$ equation.

4 Conclusions

The propagation of kovaton and compacton of the $K(\cos)$ equation has been studied by means of a new Padé numerical method. The good accuracy of the numerical method has been assessed by means of the error in the solution and the invariants for the propagation of compactons and kovatons. For compactons, small forward and backward wavepackets of radiation with a clear self-similar shape have been reported; the speed of the wave fronts of both radiations have been determined, being constant and independent of the grid spacing and time step of the numerical method. For kovatons, the main sources of the numerical error in the solution are the appearance of a small residual at the falling kink, whose area depends on the length of plateau, and the emission of a backward, square-like pulse whose length is also similar to that of the plateau.

The study of the collisions between compactly supported, solitary waves of the $K(\cos)$ equation requires the addition of small artificial viscosity for stability, as in the case of the $K(n, n)$ equation. For compactons, the collisions are very similar in both equations, showing a small amplitude residual decomposing in compacton-antcompacton pairs. The interaction between a compacton and a kovaton with a large enough plateau shows that the compacton passes through the rising kink, then it travels reversed like an antcompacton along the plateau, until reaching the falling kink of the kovaton, when it reemerges with its original shape. After the interaction two small residuals are generated, which decomposes in trains of compacton-antcompacton pairs. Finally, the collisions between antcompactons and compactons result in the blow up of the solution due to the grow up in amplitude of dispersive shock-like structures in the solution.

Present results show the great interest of the numerical study of the interactions of compactly supported solitary waves of generalizations of the $K(n, n)$ equation, as those presented in Ref. [16], since only a few have been numerically studied in detail. Furthermore, the use of other numerical methods, like finite volume methods for nonconvex conservation laws, is promising since the presence of shock-like phenomena can be considered a common feature of all the evolution equations with nonlinear dispersion.

Acknowledgments

The research reported here was partially supported by Projects MTM2010–19969 and TIN2008–05941 of the Ministerio de Ciencia e Innovación of Spain, and by Project TIC-6083 of the Consejería de Economía, Innovación y Ciencia

of the Junta de Andalucía.

References

- [1] P. Rosenau, J. M. Hyman, Compactons: Solitons with finite wavelength, *Phys. Rev. Lett.* 70 (1993) 564–567.
- [2] A. Khare and F. Cooper, One-parameter family of soliton solutions with compact support in a class of generalized Korteweg-de Vries equations, *Phys. Rev. E* 48 (1993) 4843–4844.
- [3] F. Cooper, H. Shepard, P. Sodano, Solitary waves in a class of generalized Korteweg-de Vries equations, *Phys. Rev. E* 48 (1993) 4027–4032.
- [4] F. Cooper, J. M. Hyman and A. Khare, Compacton solutions in a class of generalized fifth-order Korteweg-de Vries equations, *Phys. Rev. E* 64 (2001) 026608.
- [5] A. Chertock, D. Levy, Particle methods for dispersive equations, *J. Comput. Phys.* 171 (2001) 708–730.
- [6] M. S. Ismail, T. R. Taha, A numerical study of compactons, *Math. Comput. Simul.* 47 (1998) 519–530.
- [7] F. Rus, F.R. Villatoro, Numerical methods based on modified equations for nonlinear evolution equations with compactons, *Appl. Math. Comput.* 204 (2008) 416–422.
- [8] J. de Frutos, M. A. López-Marcos, J. M. Sanz-Serna, A finite difference scheme for the $K(2, 2)$ compacton equation, *J. Comput. Phys.* 120 (1995) 248–252.
- [9] J. Garralón, F. Rus, F.R. Villatoro, Compacton numerically-induced radiation in a fourth-order finite element method, *WSEAS Trans. Math.* 5 (2006) 89–96.
- [10] F. Rus, F.R. Villatoro, Time-stepping in Petrov-Galerkin methods based on cubic B-splines for compactons, *Appl. Math. Comput.* 217 (2010) 2788–2797.
- [11] F. Rus, F.R. Villatoro, Padé numerical method for the Rosenau–Hyman compacton equation, *Math. Comput. Simul.* 76 (2007) 188–192.
- [12] B. Mihaila, A. Cardenas, F. Cooper, A. Saxena, Stability and dynamical properties of Rosenau–Hyman compactons using Padé approximants, *Phys. Rev. E* 81 (2010) 056708.
- [13] F. Rus, F.R. Villatoro, Self-similar radiation from numerical Rosenau–Hyman compactons, *J. Comput. Phys.* 227 (2007) 440–454.
- [14] F. Rus, F.R. Villatoro, Adiabatic perturbations for compactons under dissipation and numerically-induced dissipation, *J. Comput. Phys.* 228 (2009) 4291–4302.

- [15] A. Cardenas, B. Mihaila, F. Cooper, A. Saxena, Properties of compacton-antcompacton collision, *Phys. Rev. E* 83 (2011) 066705.
- [16] F. Rus, F.R. Villatoro, A repository of equations with cosine/sine compactons, *Appl. Math. Comput.* 215 (2009) 1838–1851.
- [17] P. Rosenau, A. Pikovsky, Phase compactons in chains of dispersively coupled oscillators, *Phys. Rev. Lett.* 94 (2005) 174102.
- [18] A. Pikovsky, P. Rosenau, Phase compactons, *Physica D* 218 (2006) 56.
- [19] Synchronization: A Universal Concept in Nonlinear Science, “*Cambridge Univ. Press, Cambridge*,” (A. Pikovsky, M. Rosenblum, J. Kurths) 2001.
- [20] K. Ahnert, A. Pikovsky, Traveling waves and compactons in phase oscillator lattices, *Chaos* 18 (2008) 37118.
- [21] N. J. Balmforth, Solitary Waves and Homoclinic Orbits, *Annu. Rev. Fluid Mech.* 27 (1995) 335-373.
- [22] J. Garraón and F.R. Villatoro, Numerical evaluation of compactons and kovatons of the Rosenau–Pikovsky equation, *Math. Comp. Model.* 55 (2012) 1858–1865.
- [23] Dynamics of Josephson Junctions and Circuits, “*Gordon Breach Sci Publ Ltd, Philadelphia*,” (K.K. Likharev) 1991.
- [24] A. Vilfan, Th. Duke, Frequency Clustering in Spontaneous Otoacoustic Emissions from a Lizard’s Ear, *Biophys. J.* 95 (2008) 4622-4630.
- [25] M. Destrade, P. M. Jordan, G. Saccomandi, Compact travelling waves in viscoelastic solids, *Europhys. Lett.* 87 (2009) 48001.
- [26] G. Saccomandi, I. Sgura, The relevance of nonlinear stacking interactions in simple models of double-stranded DNA, *J. R. Soc. Interface* 3 (2006) 655–667.
- [27] J. C. Comte, P. Marquié, Compact-like kink in a real electrical reaction-diffusion chain, *Chaos, Solitons Fractals* 29 (2006) 307–312.